# Imaging of $\alpha_v\beta_3$ Expression by a Bifunctional Chimeric RGD Peptide not Cross-Reacting with $\alpha_v\beta_5$

Antonella Zannetti,[1] Silvana Del Vecchio,[1,2] Francesca Iommelli,[1] Annarita Del Gatto,[1] Stefania De Luca,[1] Laura Zaccaro,[1] Angela Papaccioli,[1] Jvana Sommella,[1] Mariarosaria Panico,[1] Antonio Speranza,[1] Paolo Grieco,[3] Ettore Novellino,[3] Michele Saviano,[1] Carlo Pedone,[1] and Marco Salvatore[1,2]

**Abstract**

**Purpose**: To test whether a novel bifunctional chimeric peptide comprising a cyclic Arg-Gly-Asp pentapeptide covalently bound to an echistatin domain can discriminate $\alpha_v\beta_3$ from $\alpha_v\beta_5$ integrin, thus allowing the *in vivo* selective visualization of $\alpha_v\beta_3$ expression by single-photon and positron emission tomography (PET) imaging.

**Experimental Design:** The chimeric peptide was preliminarily tested for inhibition of $\alpha_v\beta_3$-dependent cell adhesion and competition of $^{125}$I-echistatin binding to membrane of stably transfected K562 cells expressing $\alpha_v\beta_3$ ($K\alpha_v\beta_3$) or $\alpha_v\beta_5$ ($K\alpha_v\beta_5$) integrin. The chimeric peptide was then conjugated with diethylenetriaminepentaacetic acid and labeled with $^{111}$In for single-photon imaging, whereas a one-step procedure was used for labeling the full-length peptide and a truncated derivative, lacking the last five C-terminal amino acids, with $^{18}$F for PET imaging. Nude mice bearing tumors from $K\alpha_v\beta_3$, $K\alpha_v\beta_5$, U87MG human glioblastoma, and A431 human epidermoid cells were subjected to single-photon and PET imaging.

**Results:** Adhesion and competitive binding assays showed that the novel chimeric peptide selectively binds to $\alpha_v\beta_3$ integrin and does not cross-react with $\alpha_v\beta_5$. In agreement with *in vitro* findings, single-photon and PET imaging studies showed that the radiolabeled chimeric peptide selectively localizes in tumor xenografts expressing $\alpha_v\beta_3$ and fails to accumulate in those expressing $\alpha_v\beta_5$ integrin. When $^{18}$F-labeled truncated derivative was used for PET imaging, $\alpha_v\beta_3$- and $\alpha_v\beta_5$-expressing tumors were visualized, indicating that the five C-terminal amino acids are required to differentially bind the two integrins.

**Conclusion:** Our findings indicate that the novel chimeric Arg-Gly-Asp peptide, having no cross-reaction with $\alpha_v\beta_5$ integrin, allows highly selective $\alpha_v\beta_3$ expression imaging and monitoring. (Clin Cancer Res 2009;15(16):5224–33)



Integrins are heterodymeric membrane glycoproteins composed of noncovalently associated $\alpha$ and $\beta$ subunits that promote cell attachment and migration on the surrounding extracellular matrix. Many integrins bind to their extracellular ligands through the recognition of the tripeptide Arg-Gly-Asp (RGD). This motif is present in several protein components of extracellular matrix, including vitronectin, fibronectin, osteopontin, and fibrinogen. Although different ligands can bind to the same integrin, sequences flanking the RGD peptide are reported to be important for integrin selectivity (1). Integrin ligation by its own natural ligands promotes intracellular signaling by coclustering with kinases and adaptor proteins and by activating a number of intracellular mediators that ultimately lead to cell migration, survival, and invasion (2, 3). Interestingly, loss of integrin ligation can initiate apoptosis independently of cell attachment (4).

Among members of the integrin family, a prominent role in angiogenesis and metastatic dissemination is played by $\alpha_v\beta_3$ and $\alpha_v\beta_5$. Despite the fact that both integrins bind to vitronectin receptor and participate in the same processes, they are reported to mediate preferential responses to distinct angiogenic growth factors and signaling. *In vivo* angiogenesis assays provided indeed evidence that $\alpha_v\beta_3$ is required for basic fibroblast growth factor–induced angiogenesis, whereas vascular endothelial growth factor–induced angiogenesis mainly depends on $\alpha_v\beta_5$ (5, 6). Although recent studies indicate a more complex arrays

**Authors' Affiliations:** [1]Institute of Biostructures and Bioimages, National Research Council, and Departments of [2]Biomorphological and Functional Sciences and [3]Pharmaceutical Chemistry and Toxicology, University of Naples "Federico II," Naples, Italy

Received 12/22/08; revised 5/8/09; accepted 5/8/09; published OnlineFirst 8/11/09.

**Grant support:** European Union grant European Molecular Imaging Laboratories Network contract 503569, Ministero dell'Universita' e della Ricerca, and Centro Regionale di Competenza in Diagnostica e Farmaceutica Molecolari della Regione Campania.

The costs of publication of this article were defrayed in part by the payment of page charges. This article must therefore be hereby marked *advertisement* in accordance with 18 U.S.C. Section 1734 solely to indicate this fact.

**Requests for reprints:** Silvana Del Vecchio, Department of Biomorphological and Functional Sciences, University of Naples "Federico II," Edificio 10, Via S. Pansini 5, 80131 Naples, Italy. Phone: 39081-7463307; Fax: 39081-5457081; E-mail: delvecc@unina.it.



doi:10.1158/1078-0432.CCR-08-3270

### Translational Relevance

This article shows that a newly synthesized chimeric Arg-Gly-Asp peptide is able to discriminate *in vitro* and *in vivo* between $\alpha_v\beta_3$ and $\alpha_v\beta_5$ integrins. Although both integrins serve as vitronectin receptor and share a central role in angiogenesis and metastatic dissemination, they are reported to have differential signaling and transcriptional regulation. Integrin $\alpha_v\beta_3$ is strongly up-regulated in activated endothelial cells of newly formed blood vessels. Therefore, it has been proposed and used as target for imaging of angiogenesis. However, the peptides currently used for imaging of angiogenesis can bind to $\alpha_v\beta_3$ but also recognize $\alpha_v\beta_5$ integrin. The major translational relevance of this study is to provide a more selective tool that can be used for imaging of angiogenesis and for monitoring antiangiogenic therapy by positron emission tomography and single-photon emission computed tomography in cancer patients.

of intersections between the pathways mediated by $\alpha_v\beta_3$ and $\alpha_v\beta_5$, it remains to be elucidated whether some pathologic conditions characterized by abnormal blood vessel formation are mainly related to $\alpha_v\beta_3$ or $\alpha_v\beta_5$ dysfunction.

Integrins, including $\alpha_v\beta_3$ or $\alpha_v\beta_5$, are not constitutively active. They are expressed on the plasma membrane in an inactive status in which they do not bind their ligands and do not transduce signals unless exposed to activating external stimuli (7). Crystallography, nuclear magnetic resonance, and electron microscopy studies suggest indeed that the inactive status is characterized by a bent spatial conformation, whereas integrin activation is associated with an unbending and elongation of the dimers and separation of the cytoplasmatic domains. In particular, the crystal structure of the extracellular segment of integrin $\alpha_v\beta_3$ in its unligated state (8) and in complex (9) with a cyclic peptide presenting the RGD sequence shows the occurrence of both tertiary and quaternary changes in the presence of ligand. Recent studies also showed the cross-activation of $\alpha_v\beta_3$ and vascular endothelial growth factor receptor 2 through the formation of an integrin-TKR complex, which requires recruitment and activation of c-src and subsequent phosphorylation of the cytosolic tail of $\beta_3$ chain (10). Similarly, integrin $\alpha_v\beta_5$, which is constitutively expressed on vascular endothelium in an inactive spatial conformation, can be activated by vascular endothelial growth factor receptor 2–mediated signaling (11).

Integrin $\alpha_v\beta_3$ is strongly up-regulated at transcriptional level by proangiogenic growth factors or chemokines in activated endothelial cells. Expression and activation of this integrin was also found to be correlated with tumor invasion and metastases in melanomas, gliomas, ovarian, and breast cancer (12–15). In particular, activated $\alpha_v\beta_3$ is reported to cooperate with metalloproteinase and to strongly promote metastasis in human breast cancer cells (16, 17). Although less extensively studied, also, $\alpha_v\beta_5$ is reported to be involved in tumor invasion and metastases in a variety of malignant tumors mainly of epithelial origin. In this respect, $\alpha_v\beta_5$ physically interacts with urokinase plasminogen activator receptor, promoting proteolytic disruption of extracellular matrix, dysregulation of cell adhesion properties, and urokinase-dependent cell migration in breast cancer (18). Furthermore, $\alpha_v\beta_5$ is required for metastatic dissemination of carcinoma cells growing in a preirradiated stroma (19). Because of the putative differential role of $\alpha_v\beta_3$ and $\alpha_v\beta_5$ in tumor angiogenesis and metastatic dissemination, the development of new compounds capable of discriminating between $\alpha_v\beta_3$ and $\alpha_v\beta_5$ would hopefully shed light on the relative role of these integrins in tumor growth and progression.

A number of $\alpha_v\beta_3$ antagonists, including antibodies, peptidomimetics, and cyclic RGD peptides, have been developed and are currently used in clinical trials to inhibit $\alpha_v\beta_3$-mediated processes and to visualize tumor angiogenesis and metastases. Among these compounds, monoclonal antibodies, such as LM609 or its humanized version Vitaxin, can effectively discriminate between $\alpha_v\beta_3$ and $\alpha_v\beta_5$, whereas RGD-based peptides and peptidomimetics bind to both integrins, although with different affinity. For imaging purposes, antibody and peptide-based probes have been used for fluorescence (20), magnetic resonance (21, 22), ultrasound (23), single-photon emission tomography (24), and positron emission tomography (PET; refs. 25–27). However, antibody-based compounds, despite the development of chimeric, humanized, and engineered molecules, suffer of several limitations because of the long circulation half-life, the high background activity, the poor tumor penetration, and the nonuniform intratumoral distribution. For these reasons, peptide-based probes, despite the lack of absolute integrin selectivity, are preferred for imaging studies. In particular $^{18}$F-galacto-RGD showed favorable pharmacokinetics properties and has been tested in cancer patients (28, 29).

In a previous study, we designed and synthesized a novel bifunctional chimeric RGD peptide, including a cyclic RGD pentapeptide covalently linked by a spacer to an echistatin domain (RGDechi) that showed a high selectivity for $\alpha_v\beta_3$ integrin (30). In particular, we showed that RGDechi and a cyclic RGD pentapeptide of reference have a similar binding affinity for $\alpha_v\beta_3$, but they differ in that RGDechi failed to bind $\alpha_v\beta_5$ integrin. The aim of the present study was to test the ability of this chimeric peptide to discriminate *in vivo* $\alpha_v\beta_3$ from $\alpha_v\beta_5$ and to differentially modulate the function of the two integrins. To this end, the novel chimeric peptide was labeled with $^{111}$In and $^{18}$F and then used for noninvasive single-photon and PET imaging studies in nude mice bearing $\alpha_v\beta_3$- or $\alpha_v\beta_5$-expressing tumors.

## Materials and Methods

***Peptides synthesis and radiolabeling.*** The amino acid sequence of RGDechi and the other peptides used in the study are shown in Table 1. The chimeric peptide RGDechi and its linear precursors were designed as previously reported (30). To avoid the labeling in solution of a Lys$^{15}$, the RGDechi sequence was modified by substituting this amino acid with homocitrulline residue (RGDechi-hCit; Table 1). Moreover, to test whether the C-terminal residues of RGDechi are needed to specifically recognize the $\beta_3$ subunit, RGDechi1-14 peptide lacking the five C-terminal amino acids was designed. The cyclic pentapeptide c (RGDfV) was used as the main representative compound of the class of small RGD peptides. RGDechi, RGDechi linear fragments, RGDechi-hCit, RGDechi1-14, and c(RGDfV) were obtained as previously described by solid phase method (30).

Diethylenetriaminepentaacetic acid (DTPA)–RGDechi peptide was synthesized by introducing the N-terminal lysine into the sequence as

**Table 1.** Amino acid sequence and molecular weight of the newly synthesized peptides along with the correspondent radiolabeled compounds used in the imaging studies

| Peptide | Amino acid sequence | Molecular weight | Radiolabeled ligands |
|---|---|---|---|
| RGDechi | c(KRGDe)MDDPGRNPHKGPAT | 2,060.2 | [$^{111}$In-DTPA-ε-Lys$^{1}$]–RGDechi |
| RGDechi-hCit | c(KRGDe)MDDPGRNPH*hCit*GPAT | 2,102.0 | 4-[$^{18}$F]fluorobenzoyl-ε-Lys$^{1}$–RGDechi-hCit |
| RGDechi1-14 | c(KRGDe)MDDPGRNPH | 1,604.0 | 4-[$^{18}$F]fluorobenzoyl-ε-Lys$^{1}$–RGDechi1-14 |
| RGDechi linear | KRGDeMDDPGRNPHKGPAT | 2,078.2 | |
| Echi6-19 | MDDPGRNPHKGPAT | 1,492.6 | |
| Echi11-19 | RNPHKGPAT | 977.0 | |
| RGD | c(RGDfV) | 574.6 | |

Dde-Lys(Fmoc)-OH derivative to bind the chelating agent on the ε-$NH_2$ of Lys$^{1}$ selectively. The synthetic procedure to carry out this reaction was fully described (31). RGDechi was labeled with $^{111}$In for single-photon emission computed tomography imaging at a specific activity of 15 GBq/μmol. Briefly, the DTPA-RGDechi peptide was dissolved in 20% $CH_3CN$:80% $H_2O$ at concentrations of 0.1 to 1 mmol/L and incubated with 370 MBq $^{111}$In-citrate for 1 h at room temperature. Labeling efficiency was determined by reverse phase (RP) high performance liquid chromatography and was >97%.

For PET imaging studies, *N*-succinimidyl-4-[$^{18}$F]fluorobenzoate was used to label the ε-amino group of lysine in position 1 of RGDechi-hCit following the procedure described by Lang and Eckelman (32). Briefly, *N*-succinimidyl-4-[$^{18}$F]fluorobenzoate was prepared by reacting pentamethyl 4-(trimethylammoniumtrifluoromethanesulfonate) benzoate (3 mg), kindly provided by Dr. L. Lang, with anhydrous $^{18}$F-fluoride in presence of Kryptofix and potassium carbonate in acetonitrile at 105° for 10 min. The resulting pentamethyl ester was hydrolyzed with 0.1 mL trifluoroacetic acid to give 4-[$^{18}$F]fluorobenzoic acid

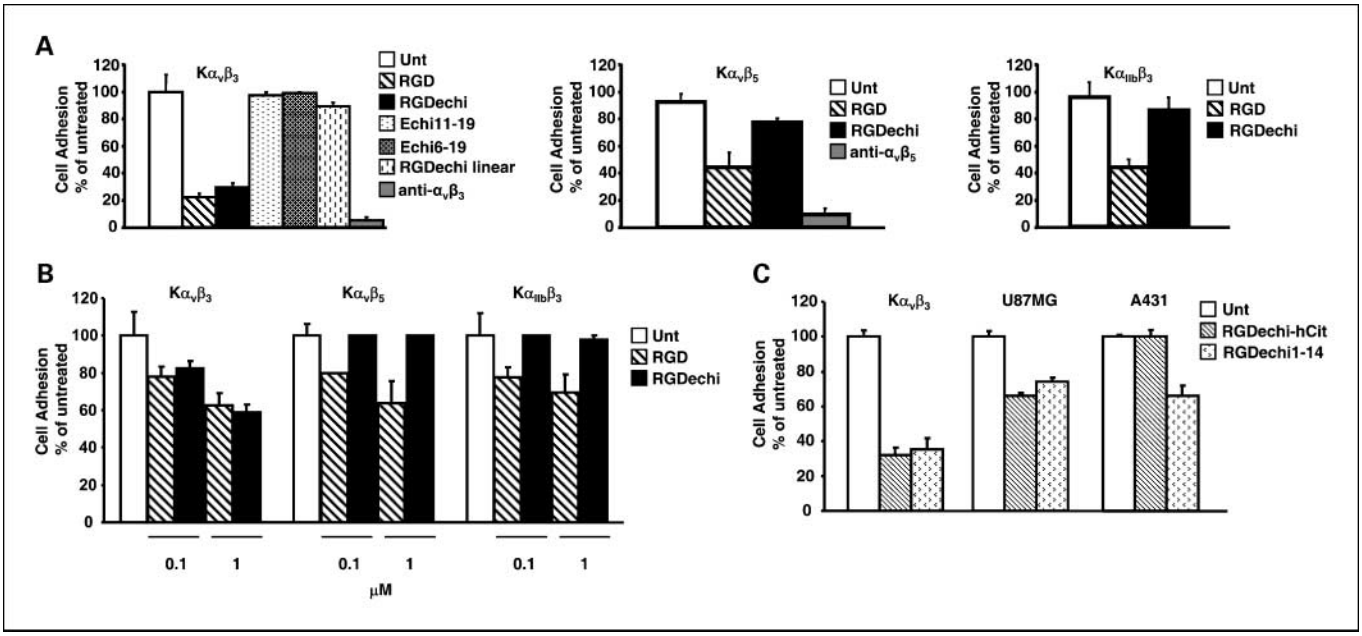


**Fig. 1.** Highly selective inhibition of $\alpha_v\beta_3$-dependent cell adhesion by the bifunctional chimeric peptide. Human erythroleukemia K562 cells alternatively expressing $\alpha_v\beta_3$ ($K\alpha_v\beta_3$), $\alpha_v\beta_5$ ($K\alpha_v\beta_5$), or $\alpha_{IIb}\beta_3$ ($K\alpha_{IIb}\beta_3$) were pretreated with the indicated peptide and then subjected to the adhesion assay. Three independent experiments were done in triplicates for each cell line, and results are expressed as percentage of adherent cells considering the untreated control cells as 100%. *A* (*left*), $K\alpha_v\beta_3$ cells were preincubated with 10 μmol/L RGD–containing peptides, 10 μmol/L fragments lacking RGD motif, 10 μg/mL anti-$\alpha_v\beta_3$ LM609, or diluents for 1 h at 4°C, and seeded on vitronectin-coated plates. The cells were allowed to adhere for 1 h at 37°C and then counted. RGDechi and cyclic RGD pentapeptide were able to significantly inhibit adhesion of $K\alpha_v\beta_3$ cells to vitronectin ($P < 0.01$), whereas echi11-19, echi6-19, and linear RGDechi failed to inhibit cell adhesion. Anti-$\alpha_v\beta_3$ LM609 monoclonal antibody, used as positive control, almost completely blocked cell adhesion. Middle, $K\alpha_v\beta_5$ cells were incubated with 10 μmol/L RGD-containing peptides, 10 μg/mL anti-$\alpha_v\beta_5$ P1F6, or diluents for 1 h at 4°C, and seeded on vitronectin-coated plates. RGDechi did not show any significant inhibitory effect on adhesion of $K\alpha_v\beta_5$ cells, indicating a lack of peptide cross-reactivity with $\alpha_v\beta_5$ integrin. Conversely, the cyclic RGD pentapeptide and anti $\alpha_v\beta_5$ P1F6 monoclonal antibody caused a 53% and 90% reduction of cell adhesion to vitronectin, respectively ($P < 0.05$). Right, $K\alpha_{IIb}\beta_3$ cells, preincubated with LM609 monoclonal antibody to avoid any interference of $\alpha_v\beta_3$, were treated with 10 μmol/L RGDechi and cyclic RGD pentapeptide, as described above, and allowed to adhere to fibrinogen-coated plates. Cell adhesion was not significantly inhibited by RGDechi, indicating that the chimeric peptide does not cross-react with $\alpha_{IIb}\beta_3$ integrin. Conversely, the cyclic RGD pentapeptide caused 56% reduction of cell adhesion ($P = 0.05$). *B,* the cell adhesion assay was done in $K\alpha_v\beta_3$, $K\alpha_v\beta_5$, and $K\alpha_{IIb}\beta_3$ cells using 0.1 and 1 μmol/L of RGDechi and cyclic RGD pentapeptide. Both peptides inhibited $K\alpha_v\beta_3$ cell adhesion in a dose-dependent manner. No effect of RGDechi on cell adhesion was observed in $K\alpha_v\beta_5$ and $K\alpha_{IIb}\beta_3$ cells, whereas the RGD pentapeptide showed a reduction of cell adhesion in $K\alpha_v\beta_5$ and $K\alpha_{IIb}\beta_3$ cells even at these lower concentrations. *C,* to test the ability of full-length RGDechi and its truncated derivative to inhibit $\alpha_v\beta_3$- and $\alpha_v\beta_5$-dependent cell adhesion, U87MG and A431 cells were pretreated with 10 μmol/L of RGDechi-hCit or RGDechi1-14, lacking the last five C-terminal amino acids, and then subjected to the adhesion assay, as described above. $K\alpha_v\beta_3$ cells were used for comparison. Both peptides were able to inhibit adhesion of $K\alpha_v\beta_3$ and U87MG cells to vitronectin, although to a different extent in the two cell lines. Conversely, RGDechi-hCit did not have any effect on adhesion of A431 cells, whereas the truncated derivative decreased A431 adhesion by a percentage similar to that obtained in U87MG.

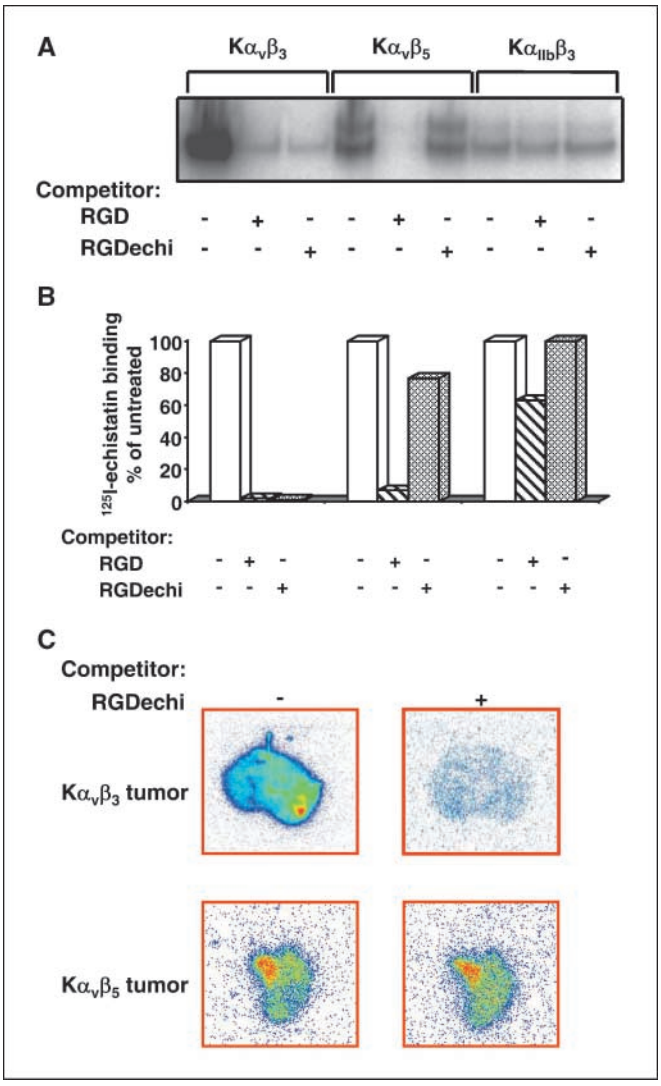


**Fig. 2.** Inhibition of $^{125}$I-echistatin binding to $\alpha_v\beta_3$ by the bifunctional chimeric peptide. *A*, membrane fractions of $K\alpha_v\beta_3$, $K\alpha_v\beta_5$, and $K\alpha_{IIb}\beta_3$ cells (100 μg) were incubated with $^{125}$I-echistatin in the presence or absence of a large molar excess of unlabeled RGDechi or cyclic RGD pentapeptide. The samples were analyzed by nondenaturing 3% to 8% SDS-PAGE under nonreducing conditions and revealed by autoradiography. SDS-stable complexes containing $^{125}$I-echistatin and RGD-binding integrins were found in membranes from $K\alpha_v\beta_3$, $K\alpha_v\beta_5$, and $K\alpha_{IIb}\beta_3$ cells in the absence of any competitor. RGDechi and RGD pentapeptide were able to compete for the binding of $^{125}$I-echistatin to $\alpha_v\beta_3$ in $K\alpha_v\beta_3$ cells. RGDechi did not compete with $^{125}$I-echistatin for the binding to $\alpha_v\beta_5$ and $\alpha_{IIb}\beta_3$ integrins in $K\alpha_v\beta_5$ and $K\alpha_{IIb}\beta_3$ cells, respectively. Conversely, the cyclic RGD pentapeptide completely abolished $^{125}$I-echistatin binding to $\alpha_v\beta_5$ integrin and caused a reduction of $^{125}$I-echistatin–$\alpha_{IIb}\beta_3$ integrin complexes. *B*, autoradiograms from SDS-PAGE were subjected to quantitative analysis using a phosphoimager, and radioactivity in each band was expressed as a percentage of that found in the absence of competitor. *C*, 8-μm frozen sections were obtained from $\alpha_v\beta_3$ or $\alpha_v\beta_5$ xenografts, incubated with $^{125}$I-echistatin in the presence or absence of a large excess of unlabeled RGDechi, and exposed to phosphor imaging plates. Images were then analyzed using the computerized imaging system. RGDechi completely abolished the binding of $^{125}$I-echistatin to sections of $\alpha_v\beta_3$-expressing tumors but was unable to compete for the binding of disintegrin to $\alpha_v\beta_5$-expressing tumors.

that was converted to *N*-succinimidyl-4-[$^{18}$F]fluorobenzoate using *N*,*N*′-disuccinimidyl carbonate. After purification, *N*-succinimidyl-4-[$^{18}$F]fluorobenzoate was incubated with 50 μg RGDechi-hCit in a phosphate buffer solution (pH 7.1) at room temperature for 20 to 60 min until most of *N*-succinimidyl-4-[$^{18}$F]fluorobenzoate had reacted as assessed by gradient analytic high performance liquid chromatography. The same procedure was used to label the truncated version of the same peptide, RGDechi1-14, lacking the five C-terminal amino acids (Table 1). The specific activity of the radiolabeled product was estimated to be on average 277 GBq/μmol.

***Cell lines and culture conditions.*** Human erythroleukemia K562 cells, stably cotransfected with cDNA of $\alpha_v$ or $\alpha_{IIb}$ subunits and $\beta_3$ or $\beta_5$ subunits (30) and alternatively expressing $\alpha_v\beta_3$ ($K\alpha_v\beta_3$), $\alpha_v\beta_5$ ($K\alpha_v\beta_5$), or $\alpha_{IIb}\beta_3$ ($K\alpha_{IIb}\beta_3$) (33) were a generous gift of Dr. S.D. Blystone and were grown in Iscove's modified Dulbecco's medium (Gibco Life Technologies). Human glioblastoma U87MG cells, endogenously expressing moderate levels of $\alpha_v\beta_3$ and undetectable levels of $\alpha_v\beta_5$, and human epidermoid A431 cells, expressing moderate levels $\alpha_v\beta_5$ and undetectable levels of $\alpha_v\beta_3$, were grown in DMEM (Gibco Life Technologies). Expression of $\alpha_v\beta_3$, $\alpha_v\beta_5$ and $\alpha_{IIb}\beta_3$ in all cell lines was analyzed by flow cytometry using fluorescein-isothiocyanate (FITC)-labeled LM609 (Chemicon International), P1F6 (Chemicon International), and A2A9/6 (Santa Cruz Biotechnology) monoclonal antibodies, respectively. Briefly, $5 \times 10^4$ cells were incubated for 1 h at 4°C with 5 μg/mL of FITC-conjugated mouse antibodies, then washed, resuspended, and finally analyzed by a Becton-Dickinson FACScan flow cytometer.

***Cell adhesion assay.*** Tumor cells were pretreated with the peptides listed in Table 1 and then subjected to the adhesion assay. Briefly, 24-well flat-bottom plates were incubated overnight with 5 μg/mL vitronectin or 10 μg/mL fibrinogen. Cells were incubated with 0.1 to 10 μM RGD-containing peptides, fragments without RGD motif, 10 μg/mL anti-$\alpha_v\beta_3$ LM609, 10 μg/mL anti-$\alpha_v\beta_5$ P1F6, or diluents for 1 h at 4°C. Then, cells ($2\text{-}5 \times 10^5$ cells/100 μL/well) were seeded onto precoated plates and allowed to adhere to vitronectin or fibrinogen for 1 h at 37°C in 5% $CO_2$. Nonadherent cells were removed with gentle washing, whereas adherent cells were detached by trypsinization and counted. Three independent adhesion assays were done in triplicates and results were expressed as percentage of adherent cells considering the untreated control cells as 100%.

***Membrane and tissue binding assay.*** Membrane fractions were prepared from $K\alpha_v\beta_3$, $K\alpha_v\beta_5$, and $K\alpha_{IIb}\beta_3$ cells, as described elsewhere (34), and 100 μg samples were incubated with $^{125}$I-echistatin (230,000 cpm; specific activity, 2,000 Ci/mmol) in the presence or absence of a large molar excess of unlabeled competitors (1 mmol/L) overnight at 4°C. Then, they were suspended in nonreducing SDS sample buffer (containing 100 mmol/L Tris-HCl, pH 6.8; 30% glycerol; 6% SDS; and 0.15% bromophenol blue; without β-mercaptoethanol), diluted 10-fold, and separated by 3% to 8% nondenaturing SDS-PAGE, followed by autoradiography using a computerized imaging analysis system (BAS 5000 Bio-Imaging Analyzer, Fuji Photo Film Co.G, Ltd.). In particular, SDS-stable complexes containing $^{125}$I-echistatin and RGD-binding integrins were visualized on digital images; regions of interest were drawn around the corresponding bands, and radioactivity was expressed as a percentage of that found in the absence of competitor.

Surgically removed tumors were frozen in liquid nitrogen; adjacent 8-μm sections were cut and subjected to *in vitro* binding assay, as previously described (35). Briefly, the sections were fixed in a solution of 0.25% glutaraldehyde, incubated with a blocking buffer, washed in cold PBS, and finally incubated with $^{125}$I-echistatin for 2 h at 22°C in the presence or absence of a large molar excess of unlabeled RGDechi (5 mmol/L). The tumor sections were simultaneously exposed to phosphor imaging plates, and then, images were analyzed using the computerized imaging system.

***Imaging studies in nude mice.*** Male BALB/c (*nu/nu*) mice, 6 wk old, weighing 15 to 20 g, were purchased from Charles River Laboratories. All animal experiments were approved by the local Animal Care and Use Committee. $K\alpha_v\beta_3$, $K\alpha_v\beta_5$, U87MG, or A431 cells ($5 \times 10^6$) were resuspended in 200 μL DMEM and injected s.c. into flanks of mice. Cells were allowed to grow for 2 to 3 wk, and tumors with a diameter ranging between 0.3 and 1 cm were obtained.

Tumor-bearing mice were then subjected to both single-photon imaging and microPET/CT studies using $^{111}$In- and $^{18}$F-labeled RGDechi

peptides, respectively. Briefly, 18.5 MBq of $^{111}$In-DTPA-RGDechi were i.v. injected through the tail vein. Animals were then anaesthetized, and images were obtained at 2 h postinjection using a dual-head single-photon emission computed tomography γ-camera (Siemens), equipped with medium-energy, high-resolution collimators.

A microPET/CT scanner (eXplore Vista Pre-Clinical PET Scanner, GE Healthcare) was used for PET studies. Briefly, 9 MBq of 4-[$^{18}$F]fluorobenzoyl–RGDechi-hCit or 4-[$^{18}$F]fluorobenzoyl–RGDechi1-14 were i.v. injected; animals were anesthetized at 50 min postinjection and firstly subjected to CT scan. One-bed position including the tumor was scanned (axial field of view, 68 mm), and images were acquired with the X-ray source set at 35 kVp and 200 μA. PET images were then acquired at 1 h postinjection for a total acquisition time of 30 min. The data were acquired in list mode, and the images were reconstructed by a combined algorithm based on Fourier rebinning followed by 2D iterative image reconstruction using ordered-subsets expectation maximization. The PET and CT data sets were then processed to obtain transaxial, coronal, and sagittal fusion images.

To confirm the specificity of *in vivo* uptake of 4-[$^{18}$F]fluorobenzoyl–RGDechi-hCit and 4-[$^{18}$F]fluorobenzoyl–RGDechi1-14, blocking studies with a large excess of unlabeled peptides were done in nude mice bearing U87MG or A431 tumors. Briefly, animals underwent a first PET/CT study using $^{18}$F-labeled peptide, and after 24 to 48 h, they were pretreated with 10 mg/kg of unlabeled correspondent peptide and then subjected to a second PET/CT scan with the same $^{18}$F-labeled peptide. In addition, subgroups of animals bearing U87MG ($n$ = 4) and A431 ($n$ = 4) xenografts were subjected to biodistribution studies 90 min after the i.v. injection of 0.74 MBq of 4-[$^{18}$F]fluorobenzoyl–RGDechi-hCit. The animals were sacrificed by cervical dislocation, and tumor, blood, and major organs, including heart, liver, spleen, lung, and kidneys were collected, wet weighed, and counted in a gamma counter. Tumor and organ uptake was expressed as the percentage of injected dose per gram tissue.

***Immunohistochemistry.*** Immunohistochemistry was done using the following monoclonal antibodies: anti-human integrin $\alpha_v\beta_3$ (LM609, Chemicon), anti-human integrin $\alpha_v\beta_5$ (P1F6, Chemicon), and rat anti-mouse CD31 (MEC13.3, BD Pharmingen). Consecutive frozen tumor sections (6 μm) were incubated overnight at 4°C with the primary antibody, followed by biotinylated secondary antibodies, and signal was revealed using immunoperoxidase detection system (Millipore Corporation) and diaminobenzidine as chromogen. Tumor sections were then counterstained with hematoxylin and examined by light microscopy. Intratumoral blood microvessels were counted in at least 10 regions of each CD31-stained section using a 20× magnification, and the results were expressed as the mean number of microvessels per field in a section.

***Statistics.*** Unpaired Student's $t$ test was used as appropriate. Differences between means were considered statistically significant for $P < 0.05$.

## Results

***Binding properties of bifunctional chimeric peptide and differential modulation of $\alpha_v\beta_3$ and $\alpha_v\beta_5$.*** To preliminarily test whether RGDechi was able to discriminate between $\alpha_v\beta_3$ and $\alpha_v\beta_5$, tumor cells expressing $\alpha_v\beta_3$ ($K\alpha_v\beta_3$) or $\alpha_v\beta_5$ ($K\alpha_v\beta_5$) were treated with saturating concentrations (10 μmol/L) of different peptides (Table 1), and inhibition of cell adhesion to vitronectin-coated plates was assayed. When $K\alpha_v\beta_3$ cells were treated with RGDechi, their adhesion to vitronectin was dramatically reduced as compared with untreated control cells (Fig. 1A, *left*; $P < 0.01$). Similar results were obtained with cyclic RGD pentapeptide ($P < 0.01$), and as expected, anti $\alpha_v\beta_3$ LM609 monoclonal antibody almost completely blocked cell adhesion ($P < 0.01$). Conversely, incubation with fragments of the same peptide lacking RGD motif, such as echi11-19, echi6-19, or RGDechi in its linear structure, failed to inhibit cell adhesion, which remained 97.5%, 99.0%, and 89.5% compared with that of untreated control cells, respectively (Fig. 1A, *left*). When $K\alpha_v\beta_5$ cells were treated with 10 μmol/L RGDechi, no significant reduction of cell adhesion to vitronectin was observed as compared with untreated control cells (Fig. 1A, *middle*), indicating that RGDechi cannot bind to and modulate the function of $\alpha_v\beta_5$ integrin. On contrast, the cyclic RGD pentapeptide caused a 53% reduction of cell adhesion to vitronectin ($P < 0.02$), and an even greater reduction (90%) of cell adhesion was caused by treatment with anti-$\alpha_v\beta_5$ P1F6 monoclonal antibody used as positive control ($P < 0.01$).

Because $\alpha_{IIb}\beta_3$ integrin, expressed at high density on platelets, recognizes the RGD motif and upon its ligation promotes platelets aggregation, we wanted to exclude that RGDechi could cross-react with this integrin. Therefore, similar adhesion assays were done in $K\alpha_{IIb}\beta_3$ cells expressing $\alpha_{IIb}\beta_3$ integrin. Cells were

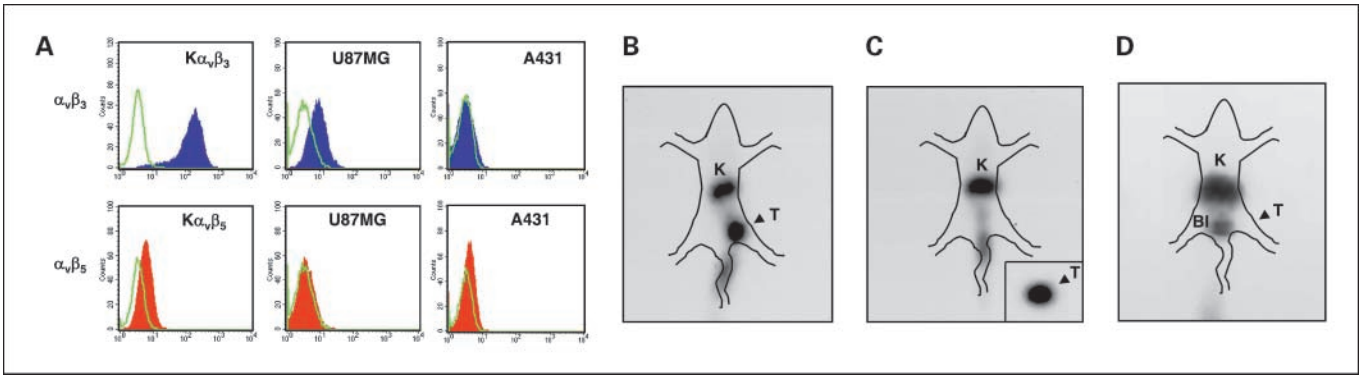


**Fig. 3.** Relative levels of $\alpha_v\beta_3$ and $\alpha_v\beta_5$ integrins in the cell lines used for imaging studies and selective *in vivo* localization of $^{111}$In-labeled chimeric peptide in $\alpha_v\beta_3$-expressing tumors. *A,* the relative levels of $\alpha_v\beta_3$ and $\alpha_v\beta_5$ integrins were analyzed by flow cytometry using FITC-labeled LM609 (*blue-filled histograms*), P1F6 (*red-filled histograms*), or irrelevant monoclonal antibodies (*open histograms*). Levels of $\alpha_v\beta_3$ (*top*) were higher in $K\alpha_v\beta_3$ than in U87MG, whereas the same integrin was virtually absent in A431 cells. Conversely, the relative levels of $\alpha_v\beta_5$ (*bottom*) were higher in $K\alpha_v\beta_5$ cells than in A431 cells and undetectable in U87MG cells. *B,* nude mice bearing xenografts from $K\alpha_v\beta_3$ or $K\alpha_v\beta_5$ cells were subjected to single-photon imaging 2 h after injection of $^{111}$In-DTPA-RGDechi through the tail vein, and representative images are shown. $\alpha_v\beta_3$-Expressing tumor showed a high tumor uptake of the tracer. *C,* to confirm the high uptake of $\alpha_v\beta_3$ xenograft, tumor was removed from the sacrificed animal, and both were subjected to single-photon imaging. Inset, excised $\alpha_v\beta_3$ tumor. *D,* nude mice bearing $K\alpha_v\beta_5$ tumors were subjected to single-photon imaging, as described in *B*. $^{111}$In-labeled chimeric peptide failed to accumulate in $\alpha_v\beta_5$-expressing tumors. K, kidney; Bl, bladder; T, tumor.

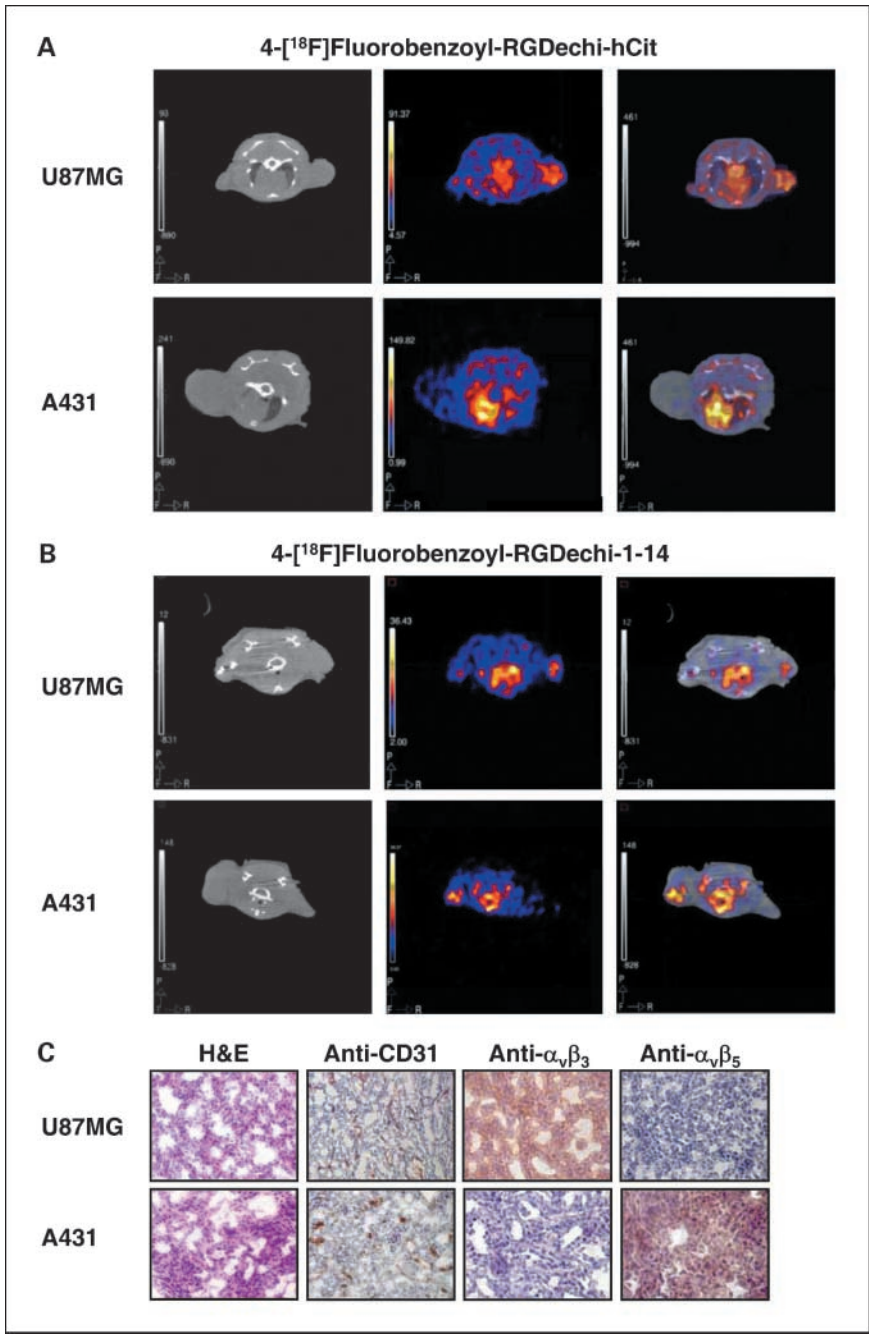


**Fig. 4.** Imaging of $\alpha_v\beta_3$-expressing tumors by $^{18}$F-labeled chimeric peptides and microPET/CT. *A,* nude mice bearing U87MG and A431 xenografts expressing either $\alpha_v\beta_3$ or $\alpha_v\beta_5$ integrins, respectively, were subjected to microPET/CT using 4-[$^{18}$F]fluorobenzoyl–RGDechi-hCit. Representative transaxial sections of CT (*left*), PET (*middle*), and corresponding fusion images (*right*) obtained 1 h after injection of 4-[$^{18}$F]fluorobenzoyl–RGDechi-hCit through the tail vein of animals bearing U87MG tumors (*top*) or A431 tumors (*bottom*). Tumor uptake of $^{18}$F-labeled chimeric peptide was observed in $\alpha_v\beta_3$-expressing U87MG xenografts, whereas $\alpha_v\beta_5$-expressing A431 tumors, despite the large size, did not accumulate the tracer. *B,* nude mice bearing U87MG and A431 xenografts were subjected to microPET/CT using 4-[$^{18}$F]fluorobenzoyl–RGDechi1-14, lacking the five C-terminal amino acids of the chimeric peptide sequence. Representative transaxial sections of CT (*left*), PET (*middle*), and corresponding fusion images (*right*) obtained 1 h after injection of 4-[$^{18}$F] fluorobenzoyl–RGDechi1-14. $\alpha_v\beta_3$- and $\alpha_v\beta_5$-expressing tumors were visualized, indicating that the last five amino acids are required by the chimeric peptide to discriminate between $\alpha_v\beta_3$ and $\alpha_v\beta_5$ integrins. *C,* after sacrifice of mice, tumors were removed and subjected to immunoperoxidase staining using rat anti-mouse CD31, anti-human integrin $\alpha_v\beta_3$ (LM609), and anti-human integrin $\alpha_v\beta_5$ (P1F6) monoclonal antibodies. Parallel sections were also stained with H&E for comparison. U87MG tumors showed a high expression of $\alpha_v\beta_3$ and undetectable levels of $\alpha_v\beta_5$, whereas A431 tumors showed positive staining for $\alpha_v\beta_5$ and no signals for $\alpha_v\beta_3$. Conversely, the two tumor models showed a similar pattern of staining with anti-CD31 and blood microvessel density was not significantly different.

preincubated with LM609 monoclonal antibody to avoid any interference of $\alpha_v\beta_3$, then treated with 10 μmol/L RGDechi and cyclic RGD pentapeptide, and allowed to adhere to fibrinogen-coated plates. Figure 1A (*right panel*) shows that RGDechi did not show any significant inhibitory effect on adhesion of $K\alpha_{IIb}\beta_3$ cells, whereas the RGD pentapeptide caused 56% reduction of cell adhesion ($P = 0.05$). Figure 1B shows the effects of lower concentrations of the two peptides on cell adhesion.

RGDechi and cyclic RGD pentapeptide at concentration of 0.1 and 1 μmol/L inhibited $K\alpha_v\beta_3$ cell adhesion in a dose-dependent manner. No effect of RGDechi on cell adhesion was observed in $K\alpha_v\beta_5$ and $K\alpha_{IIb}\beta_3$ cells, whereas the RGD pentapeptide showed a dose-dependent reduction of cell adhesion in $K\alpha_v\beta_5$ and $K\alpha_{IIb}\beta_3$ cells that was less pronounced than at saturating concentrations.

Because PET studies were done using RGDechi modified in sequence and length (Table 1), unlabeled RGDechi-hCit and RGDechi1-14 were preliminarily tested for their ability to inhibit cell adhesion in U87MG and A431 cells using $K\alpha_v\beta_3$ cells for comparison. Both peptides were able to inhibit adhesion of $K\alpha_v\beta_3$ and U87MG cells to vitronectin, although to a different extent in the two cell lines (Fig. 1C). Conversely, RGDechi-hCit did not have any effect on adhesion of A431 cells, whereas the truncated derivative (RGDechi1-14) decreased A431 adhesion by a percentage similar to that obtained in U87MG.

To further confirm the selectivity of RGDechi for $\alpha_v\beta_3$ integrin and lack of cross-reactivity with $\alpha_v\beta_5$ and $\alpha_{IIb}\beta_3$, we tested the ability of RGDechi to compete with $^{125}$I-echistatin for the binding to the selected integrins. $^{125}$I-echistatin binds to RGD-recognizing integrins and forms SDS-stable complexes in absence of chemical cross-linkers (36). Therefore, membrane fractions of $K\alpha_v\beta_3$, $K\alpha_v\beta_5$, and $K5\alpha_{IIb}\beta_3$ cells were incubated with $^{125}$I-echistatin in the presence or absence of a large molar excess of unlabeled competitors and then subjected to nondenaturing SDS-PAGE under nonreducing conditions. SDS-stable complexes containing $^{125}$I-echistatin and RGD-binding integrins were found in membranes from $K\alpha_v\beta_3$, $K\alpha_v\beta_5$, and $K\alpha_{IIb}\beta_3$ cells in the absence of any competitor (Fig. 2A). RGDechi and cyclic RGD pentapeptide were able to compete for the binding of $^{125}$I-echistatin to $\alpha_v\beta_3$ in $K\alpha_v\beta_3$ cells. Conversely, RGDechi failed to compete with $^{125}$I-echistatin for the binding to $\alpha_v\beta_5$ integrin in $K\alpha_v\beta_5$ cells, whereas RGD pentapeptide completely abolished $^{125}$I-echistatin binding to the same integrin. In $K\alpha_{IIb}\beta_3$ cells, no competition of RGDechi for $^{125}$I-echistatin binding was observed, whereas RGD pentapeptide caused a mild reduction of the intensity of the band corresponding to SDS-stable complexes. Figure 2B shows the results of the quantitative analysis done on autoradiograms and the relative intensity of each band is expressed as a percentage of corresponding untreated sample. Furthermore, the ability of RGDechi to compete for the binding of $^{125}$I-echistatin was tested on $K\alpha_v\beta_3$ and $K\alpha_v\beta_5$ xenografts that had been removed from sacrificed mice.



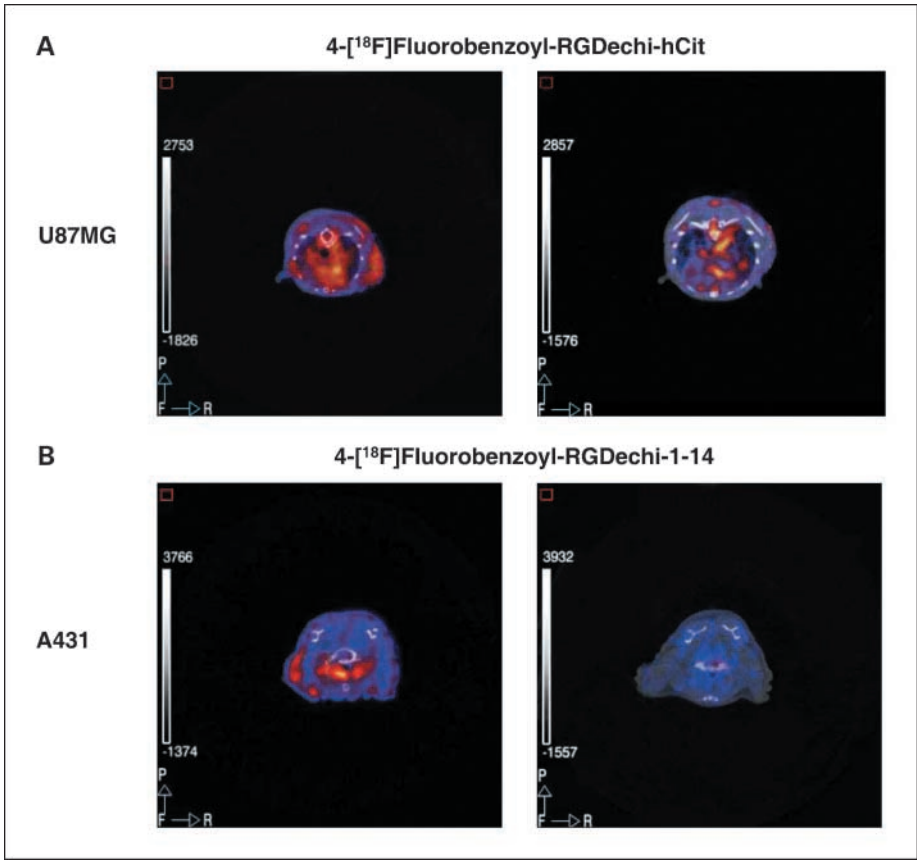


**Fig. 5.** *In vivo* blocking studies using $^{18}$F-labeled chimeric peptides and microPET/CT. Nude mice bearing U87MG (*right flank*) or A431 (*left flank*) tumors were subjected to microPET/CT using 4-[$^{18}$F]fluorobenzoyl–RGDechi-hCit or 4-[$^{18}$F]fluorobenzoyl–RGDechi1-14 with or without pretreatment with a large excess of the corresponding unlabeled peptide. *A,* representative transaxial fusion images of microPET/CT obtained 1 h after i.v. injection of 4-[$^{18}$F] fluorobenzoyl–RGDechi-hCit in U87MG tumor-bearing animal that had been pretreated (*right*) or not (*left*) with a large excess of corresponding unlabeled peptide. Excess unlabeled RGDechi-hCit prevented the binding of 4-[$^{18}$F]fluorobenzoyl–RGDechi-hCit to $\alpha_v\beta_3$-expressing tumor, indicating the specificity of the signal. *B,* representative transaxial fusion images of microPET/CT obtained 1 h after i.v. injection of 4-[$^{18}$F]fluorobenzoyl–RGDechi1-14, lacking the five C-terminal amino acids of the chimeric peptide sequence, in A431 tumor-bearing animal that had been pretreated (*right*) or not (*left*) with a large excess of corresponding unlabeled peptide. Excess unlabeled RGDechi1-14 prevented the binding of 4-[$^{18}$F]fluorobenzoyl–RGDechi1-14 to $\alpha_v\beta_5$-expressing tumor, indicating the specificity of the signal.

Frozen tumor sections were incubated with $^{125}$I-echistatin in the presence or absence of a large excess of RGDechi (Fig. 2C). Again, the chimeric peptide was able to abolish the binding of disintegrin to $\alpha_v\beta_3$ but was unable to compete for the binding of $^{125}$I-echistatin to $\alpha_v\beta_5$. Taken together, these findings show that RGDechi selectively binds to $\alpha_v\beta_3$ integrin and does not cross-react with $\alpha_v\beta_5$ and $\alpha_{IIb}\beta_3$ integrins.

***Imaging studies.*** Imaging studies were done in nude mice bearing xenografts derived from tumor cells expressing $\alpha_v\beta_3$ or $\alpha_v\beta_5$ integrin. Figure 3 shows the relative levels of both integrins in the cell lines used for *in vivo* imaging studies. Levels of $\alpha_v\beta_3$ were higher in K$\alpha_v\beta_3$ than in U87MG, whereas the same integrin was virtually absent in A431 cells (Fig. 3A, *top*). Conversely, the relative levels of $\alpha_v\beta_5$ were higher in K$\alpha_v\beta_5$ cells than in A431 cells and undetectable in U87MG cells (Fig. 3A, *bottom*).

Animals were subjected to single-photon imaging with $^{111}$In-DTPA-RGDechi and microPET/CT studies with 4-[$^{18}$F] fluorobenzoyl-labeled peptides. Representative images of tumor-bearing mice obtained 2 hours postinjection of $^{111}$In-DTPA-RGDechi are shown in Fig. 3B to D. A high tumor uptake of the tracer was observed in K$\alpha_v\beta_3$ tumors (Fig. 3B), whereas no tumor uptake could be observed in K$\alpha_v\beta_5$ tumors (Fig. 3D). To confirm the high tumor uptake, $\alpha_v\beta_3$ xenografts were surgically removed from sacrificed animals and subjected to *ex vivo* imaging (Fig. 3C).

To test whether the chimeric peptide was able to *in vivo* discriminate endogenously expressed $\alpha_v\beta_3$ and $\alpha_v\beta_5$ integrins, microPET/CT imaging studies were done in nude mice bearing U87MG and A431 tumors using 4-[$^{18}$F]fluorobenzoyl–RGDechi-hCit or its truncated form 4-[$^{18}$F]fluorobenzoyl–RGDechi1-14. Animals underwent microPET/CT 50 to 60 minutes postinjection of $^{18}$F-labeled peptides through the tail vein. Representative images of microPET/CT studies are shown in Fig. 4. Transaxial sections obtained at the level of tumors showed the localization of 4-[$^{18}$F]fluorobenzoyl–RGDechi-hCit in U87MG xenografts, whereas A431 tumors, despite their larger size, did not accumulate the tracer (Fig. 4A). When 4-[$^{18}$F]fluorobenzoyl–RGDechi1-14, lacking the five C-terminal amino acids, was injected in tumor-bearing mice, $\alpha_v\beta_3$- and $\alpha_v\beta_5$-expressing tumors were visualized, indicating that these amino acids are required by the chimeric peptide to discriminate between the two integrins (Fig. 4B). After sacrifice of mice, immunoperoxidase staining of tumor sections showed a high expression of $\alpha_v\beta_3$ in U87MG tumors and high levels of $\alpha_v\beta_5$ in A431 tumors, whereas a similar pattern of neovascularization with no significant differences in blood microvessel density was observed in the two tumor models (33 ± 7 versus 31 ± 2; Fig. 4C). Furthermore, hematoxylin and eosin staining showed no evidence of necrosis in tumor sections.

The specificity of the binding was confirmed by *in vivo* blocking studies (Fig. 5). Baseline scans showed that 4-[$^{18}$F] fluorobenzoyl–RGDechi-hCit and 4-[$^{18}$F]fluorobenzoyl–RGDechi1-14 accumulate in U87MG (Fig. 5A, *left*) and A431 tumors (Fig. 5B, *left*), respectively. This accumulation is prevented by pretreatment of animals with a large excess of the correspondent unlabeled peptide, thus indicating a specific uptake of 4-[$^{18}$F]fluorobenzoyl–RGDechi-hCit in $\alpha_v\beta_3$-expressing tumors (Fig. 5A, *right*) and 4-[$^{18}$F]fluorobenzoyl–RGDechi1-14 in $\alpha_v\beta_5$-expressing tumors (Fig. 5B, *right*).

**Table 2.** Biodistribution data of 4-[$^{18}$F] fluorobenzoyl–RGDechi-hCit expressed as percentage injected dose per gram tissue in nude mice bearing U87MG ($n$ = 4) and A431 ($n$ = 4) xenografts at 90 minutes postinjection

| Tissue | U87MG, $\alpha_v\beta_3$ positive, $\alpha_v\beta_5$ negative | A431, $\alpha_v\beta_3$ negative, $\alpha_v\beta_5$ positive |
|---|---|---|
| Tumor | 0.119 ± 0.032 | 0.022 ± 0.013 |
| Blood | 0.040 ± 0.030 | 0.019 ± 0.018 |
| Liver | 0.167 ± 0.060 | 0.140 ± 0.013 |
| Spleen | 0.007 ± 0.006 | 0.006 ± 0.006 |
| Kidneys | 0.667 ± 0.170 | 0.467 ± 0.050 |
| Lung | 0.026 ± 0.004 | 0.006 ± 0.006 |
| Stomach | 0.062 ± 0.034 | 0.030 ± 0.017 |
| Intestine | 0.166 ± 0.047 | 0.157 ± 0.007 |
| Muscle | 0.037 ± 0.034 | 0.011 ± 0.010 |
| Heart | 0.008 ± 0.007 | 0.001 ± 0.001 |
| Femur | 0.009 ± 0.009 | 0.020 ± 0.020 |

Biodistribution data obtained at a time point corresponding to the end of microPET/CT study are reported in Table 2 and showed a 5.4:1 ratio between $\alpha_v\beta_3$-expressing U87MG tumor and $\alpha_v\beta_5$-expressing A431 tumor. Tumor-to-blood ratio was 3 and 1.16 in U87MG and A431 tumors, respectively. The highest tracer uptake was observed in kidneys and liver in both animal models, whereas the activity detected in femur was negligible, indicating *in vivo* stability of the compound against defluorination. These findings taken together indicate that the chimeric peptide labeled with both γ- and positron-emitting nuclides is able to specifically localize in tumors expressing $\alpha_v\beta_3$ integrin, whereas it fails to accumulate in tumors expressing $\alpha_v\beta_5$ integrin.

## Discussion

In the present study, we showed that a newly synthesized chimeric RGD peptide is able to discriminate *in vitro* and *in vivo* between $\alpha_v\beta_3$ and $\alpha_v\beta_5$ integrins and to selectively modulate $\alpha_v\beta_3$ function. Single-photon and PET imaging studies showed indeed that the chimeric peptide labeled with either γ or positron emitters selectively localizes in tumor xenografts expressing $\alpha_v\beta_3$ and fails to accumulate in those expressing $\alpha_v\beta_5$ integrin. This ability relies upon the bifunctional nature of the peptide that contains a cyclic RGD motif linked to a fragment of the echistatin C-terminal tail. Whereas the RGD motif binds to the extracellular domain of $\alpha_v\beta_3$ but recognizes also other integrins, the C-terminal fragment of echistatin confers specificity for $\alpha_v\beta_3$, as assessed by adhesion assays and cross-linking experiments.

Previous studies showed that a number of RGD peptides can be labeled with $^{111}$In and $^{99m}$Tc for single-photon emission computed tomography imaging and with $^{18}$F, $^{64}$Cu, and $^{68}$Ga for PET imaging (37, 38). In particular, lead compounds such as $^{18}$F-galacto-RGD (25) and multimeric $^{64}$Cu-RGD peptides (39) have been developed, have been tested for their ability to detect $\alpha_v\beta_3$ integrin expression in preclinical settings, and are currently evolving into clinical trials as radiopharmaceuticals for PET studies (28, 29). According to previous studies (25), the $IC_{50}$ of $^{18}$F-galacto-RGD for inhibition of binding of

vitronectin to purified $\alpha_v\beta_3$ integrin protein fixed on a solid matrix is 5 nmol/L, whereas the same peptide inhibited vitronectin binding to purified $\alpha_v\beta_5$ with an $IC_{50}$ of 1 μmol/L, indicating a high discriminative power between the two integrins in solid phase. However, when measured in living systems wherein integrins are physiologically located in the plasma membrane and therefore can assume different spatial conformations, depending on ligand binding, and can be involved in many protein-protein interactions, the $IC_{50}$ values of cyclic RDG pentapeptides are in a much lower range of affinity and do not allow a clear-cut discrimination between $\alpha_v\beta_3$ and $\alpha_v\beta_5$, as reported by many authors (40–42). To the best of our knowledge, this is the first report on a radiolabeled chimeric RGD peptide for single-photon emission computed tomography and PET imaging that selectively binds to $\alpha_v\beta_3$ in living systems without any cross-reaction with $\alpha_v\beta_5$ even at millimolar concentrations.

In addition to the reported different signaling pathways mediated by the two integrins, $\alpha_v\beta_3$ and $\alpha_v\beta_5$ are also reported to be differentially expressed on the surface of tumor cells, especially in relation to their origin and composition of the surrounding extracellular matrix (2). Melanoma and glioblastoma cells do express high levels of $\alpha_v\beta_3$ integrin that correlate with their invasive potential. However, most epithelial-derived tumor cells do not preferentially express $\alpha_v\beta_3$ but rather use $\alpha_v\beta_5$ as vitronectin receptor (43, 44). Integrin $\alpha_v\beta_5$ was reported indeed to be expressed at moderate to high levels in most carcinoma cells, absent in lymphoma cells, and weakly expressed in myeloma cells (45, 46). In agreement with these findings, we have previously reported moderate or high levels of $\alpha_v\beta_5$ on malignant epithelial tumor cells in sections of human breast carcinomas, whereas $\alpha_v\beta_3$ expression was confined to endothelial cells of newly formed blood vessels (18), as reported also by others authors (15). Therefore, when a radiolabeled peptide cross-reacting with both integrins is used for imaging studies on $\alpha_v\beta_5$-expressing tumors, tracer accumulation at tumor sites, even if specific and displaceable by a large excess of cold ligand, may be due to the binding of peptide to $\alpha_v\beta_5$ on tumor cells and $\alpha_v\beta_3$ on endothelial cells of newly formed intratumoral blood vessels. This may have detrimental consequences when imaging is used to monitor antiangiogenic therapy because the lack of absolute selectivity of labeled peptide may obscure the endothelial cell response to these drugs.

The specificity of the binding of 4-[$^{18}$F]fluorobenzoyl–RGDechi-hCit and 4-[$^{18}$F]fluorobenzoyl–RGDechi1-14 was confirmed by *in vivo* blocking studies in which a large excess of the correspondent peptide prevented the accumulation of 4-[$^{18}$F]fluorobenzoyl–RGDechi-hCit in $\alpha_v\beta_3$-expressing U87MG tumors and 4-[$^{18}$F]fluorobenzoyl–RGDechi1-14 in $\alpha_v\beta_5$-expressing A431 xenografts. Furthermore, immunohistochemical and histopathologic findings showed that the two tumor models differ mainly for integrin expression pattern rather than for intratumoral vascularization. Therefore, the specific accumulation of chimeric $^{18}$F-labeled peptides reflects the differential pattern of integrin expression in the two tumor models rather than the differences in neovascularization. Despite the high selectivity and specificity of 4-[$^{18}$F]fluorobenzoyl–RGDechi-hCit, the absolute uptake of the tracer in U87MG tumors seemed to be suboptimal, and further studies are needed to improve its pharmacokinetics. Furthermore, in our experimental setting, the chimeric RGD peptide was not able to detect a signal originating from the newly formed intratumoral blood vessels of $\alpha_v\beta_3$ negative tumors. This may be due to incomplete neovascularization and, hence, low levels of $\alpha_v\beta_3$ expression or to the murine origin of the integrin on newly formed blood vessels because the rational design of the chimeric RGD peptide was based on the crystal structure of the extracellular region of human $\alpha_v\beta_3$ (8, 30). In agreement with *in vitro* findings, the loss of the last five C-terminal amino acids abolished the ability of the peptide to discriminate between $\alpha_v\beta_3$ and $\alpha_v\beta_5$, and the $^{18}$F-labeled truncated derivative accumulates in U87MG and A431 tumors.

In conclusion, the novel bifunctional chimeric peptide, having no cross-reaction with $\alpha_v\beta_5$ integrin, can be used for highly selective $\alpha_v\beta_3$ expression imaging by single-photon and PET technology.

## Disclosure of Potential Conflicts of Interest

No potential conflicts of interest were disclosed.

## Acknowledgments

We thank Dr. S.D. Blystone for providing cotransfected tumor cell lines, Dr. L. Lang for providing the $^{18}$F-labeling precursor, Dr. G. Pirozzi for his valuable help with fluorescent activated cell sorting (FACS) analysis, Dr. M.V. Carriero for her precious help with immunohistochemical analysis, and L. Zona and Dr. G. Perrotta for their expert technical assistance.

## References

1. Avraamides CJ, Garmy-Susini B, Varner JA. Integrins in angiogenesis and lymphangiogenesis. Nat Rev Cancer 2008;8:604–17.
2. Hood JD, Cheresh DA. Role of integrins in cell invasion and migration. Nat Rev Cancer 2002;2:91–100.
3. Guo W, Giancotti FG. Integrin signalling during tumour progression. Nat Rev Mol Cell Biol 2004;5:816–26.
4. Stupack DG, Cheresh DA. Get a ligand, get a life: integrins, signaling and cell survival. J Cell Sci 2002;115:3729–38.
5. Friedlander M, Brooks PC, Shaffer RW, Kincaid CM, Varner JA, Cheresh DA. Definition of two angiogenic pathways by distinct αv integrins. Science 1995;270:1500–2.
6. Hood JD, Frausto R, Kiosses WB, Schwartz MA, Cheresh DA. Differential αv integrin-mediated Ras-ERK signaling during two pathways of angiogenesis. J Cell Biol 2003;162:933–43.
7. Shimaoka M, Springer TA. Therapeutic antagonists and conformational regulation of integrin function. Nat Rev Drug Discov 2003;2:703–16.
8. Xiong JP, Stehle T, Diefenbach B, et al. Crystal structure of the extracellular segment of integrin αVβ3. Science 2001;294:339–45.
9. Xiong JP, Stehle T, Zhang R, et al. Crystal structure of the extracellular segment of integrin αVβ3 in complex with an Arg-Gly-Asp ligand. Science 2002;296:151–5.
10. Mahabeleshwar GH, Feng W, Reddy K, Plow EF, Byzova TV. Mechanisms of integrin-vascular endothelial growth factor receptor cross-activation in angiogenesis. Circ Res 2007;101:570–80.
11. Byzova TV, Goldman CK, Pampori N, et al. A mechanism for modulation of cellular responses to VEGF: activation of the integrins. Mol Cell 2000;6:851–60.
12. Albelda SM, Mette SA, Elder DE, et al. Integrin distribution in malignant melanoma: association of the β3 subunit with tumor progression. Cancer Res 1990;50:6757–64.
13. Schnell O, Krebs B, Wagner E, et al. Expression of integrin αvβ3 in gliomas correlates with tumor grade and is not restricted to tumor vasculature. Brain Pathol 2008;18:378–86.
14. Liapis H, Adler LM, Wick MR, Rader JS. Expression of α(v)β3 integrin is less frequent in ovarian epithelial tumors of low malignant potential in contrast to ovarian carcinomas. Hum Pathol 1997;28:443–9.
15. Gasparini G, Brooks PC, Biganzoli E, et al. Vascular integrin α(v)β3: a new prognostic indicator in breast cancer. Clin Cancer Res 1998;4:2625–34.
16. Felding-Habermann B, O'Toole TE, Smith JW, et al. Integrin activation controls metastasis in human breast cancer. Proc Natl Acad Sci U S A 2001;98:1853–8.
17. Rolli M, Fransvea E, Pilch J, Saven A, Felding-Habermann B. Activated integrin αvβ3 cooperates with metalloproteinase MMP-9 in regulating migration of metastatic breast cancer cells. Proc Natl Acad Sci U S A 2003;100:9482–7.

**18.** Carriero MV, Del Vecchio S, Capozzoli M, et al. Urokinase receptor interacts with α(v)β5 vitronectin receptor, promoting urokinase-dependent cell migration in breast cancer. Cancer Res 1999; 59:5307–14.

**19.** Monnier Y, Farmer P, Bieler G, et al. CYR61 and αVβ5 integrin cooperate to promote invasion and metastasis of tumors growing in preirradiated stroma. Cancer Res 2008;68:7323–31.

**20.** Chen X, Conti PS, Moats RA. *In vivo* near-infrared fluorescence imaging of integrin αvβ3 in brain tumor xenografts. Cancer Res 2004;64: 8009–14.

**21.** Sipkins DA, Cheresh DA, Kazemi MR, Nevin LM, Bednarski MD, Li KC. Detection of tumor angiogenesis *in vivo* by αVβ3-targeted magnetic resonance imaging. Nat Med 1998;4:623–6.

**22.** Zhang C, Jugold M, Woenne EC, et al. Specific targeting of tumor angiogenesis by RGD-conjugated ultrasmall superparamagnetic iron oxide particles using a clinical 1.5-T magnetic resonance scanner. Cancer Res 2007;67:1555–62.

**23.** Ellegala DB, Leong-Poi H, Carpenter JE, et al. Imaging tumor angiogenesis with contrast ultrasound and microbubbles targeted to α(v)β3. Circulation 2003;108:336–41.

**24.** Janssen ML, Oyen WJ, Dijkgraaf I, et al. Tumor targeting with radiolabeled α(v)β(3) integrin binding peptides in a nude mouse model. Cancer Res 2002;62:6146–51.

**25.** Haubner R, Wester HJ, Weber WA, et al. Noninvasive imaging of α(v)β3 integrin expression using 18F-labeled RGD-containing glycopeptide and positron emission tomography. Cancer Res 2001;61:1781–5.

**26.** Chen X, Hou Y, Tohme M, et al. Pegylated Arg-Gly-Asp peptide: 64Cu labeling and PET imaging of brain tumor αvβ3-integrin expression. J Nucl Med 2004;45:1776–83.

**27.** Cai W, Wu Y, Chen K, Cao Q, Tice DA, Chen X. *In vitro* and *in vivo* characterization of 64Cu-labeled Abegrin, a humanized monoclonal antibody against integrin αvβ3. Cancer Res 2006;66:9673–81.

**28.** Haubner R, Weber WA, Beer AJ, et al. Noninvasive visualization of the activated αvβ3 integrin in cancer patients by positron emission tomography and [18F]galacto-RGD. PLoS Med 2005;2:e70.

**29.** Beer AJ, Grosu AL, Carlsen J, et al. [18F]galacto-RGD positron emission tomography for imaging of αvβ3 expression on the neovasculature in patients with squamous cell carcinoma of the head and neck. Clin Cancer Res 2007;13:6610–6.

**30.** Del Gatto A, Zaccaro L, Grieco P, et al. Novel and selective α(v)β3 receptor peptide antagonist: design, synthesis, and biological behavior. J Med Chem 2006;49:3416–20.

**31.** De Luca S, Morelli G. Synthesis and characterization of a sulfated and a non-sulfated cyclic CCK8 analogue functionalized with a chelating group for metal labelling. J Pept Sci 2004;10:265–73.

**32.** Lang L, Eckelman WC. One-step synthesis of 18F labeled [18F]-*N*-succinimidyl 4-(fluoromethyl)benzoate for protein labeling. Appl Radiat Isot 1994;45:1155–63.

**33.** Blystone SD, Lindberg FP, LaFlamme SE, Brown EJ. Integrin β3 cytoplasmic tail is necessary and sufficient for regulation of α5β1 phagocytosis by αvβ3 and integrin-associated protein. J Cell Biol 1995;130:745–54.

**34.** Zannetti A, Iommelli F, Fonti R, et al. Gefitinib induction of *in vivo* detectable signals by Bcl-2/Bcl-xL modulation of inositol trisphosphate receptor type 3. Clin Cancer Res 2008;14:5209–19.

**35.** Del Vecchio S, Stoppelli MP, Carriero MV, et al. Human urokinase receptor concentration in malignant and benign breast tumors by *in vitro* quantitative autoradiography: comparison with urokinase levels. Cancer Res 1993; 53:3198–206.

**36.** Thibault G. Sodium dodecyl sulfate-stable complexes of echistatin and RGD-dependent integrins: a novel approach to study integrins. Mol Pharmacol 2000;58:1137–45.

**37.** McQuade P, Knlght LC. Radiopharmaceuticals for targeting the angiogenesis marker α(v)β(3). Q J Nucl Med 2003;47:209–20.

**38.** Beer AJ, Schwaiger M. Imaging of integrin αvβ3 expression. Cancer Metastasis Rev 2008; 27:631–44.

**39.** Wu Y, Zhang X, Xiong Z, et al. microPET imaging of glioma integrin {α}v{β}3 expression using (64)Cu-labeled tetrameric RGD peptide. J Nucl Med 2005;46:1707–18.

**40.** Goodman SL, Holzemann G, Sulyok GA, Kessler H. Nanomolar small molecule inhibitors for αv(β) 6, αv(β)5, and αv(β)3 integrins. J Med Chem 2002; 45:1045–51.

**41.** Li ZB, Chen K, Chen X. (68)Ga-labeled multimeric RGD peptides for microPET imaging of integrin α(v)β(3) expression. Eur J Nucl Med Mol Imaging 2008;35:1100–8.

**42.** Nabors LB, Mikkelsen T, Rosenfeld SS, et al. Phase I and correlative biology study of cilengitide in patients with recurrent malignant glioma. J Clin Oncol 2007;25:1651–7.

**43.** Mizejewski GJ. Role of integrins in cancer: survey of expression patterns. Proc Soc Exp Biol Med 1999;222:124–38.

**44.** Wakayama M, Abei M, Kawashima R, et al. E1A, E1B double-restricted adenovirus with RGD-fiber modification exhibits enhanced oncolysis for CAR-deficient biliary cancers. Clin Cancer Res 2007;13:3043–50.

**45.** Pasqualini R, Bodorova J, Ye S, Hemler ME. A study of the structure, function and distribution of β5 integrins using novel anti-β5 monoclonal antibodies. J Cell Sci 1993;105 (Pt 1):101–11.

**46.** Burvenich IJ, Schoonooghe S, Blanckaert P, et al. Biodistribution and planar γ camera imaging of (123)I- and (131)I-labeled F(ab')(2) and Fab fragments of monoclonal antibody 14C5 in nude mice bearing an A549 lung tumor. Nucl Med Biol 2007;34:257–65.